An Adaptive Cross-Correlation Algorithm for Extended Scene Shack-Hartmann Wavefront Sensing#

Erkin Sidick‡, Joseph J. Green, Catherine M. Ohara, and David C. Redding
Jet Propulsion Laboratory, California Institute of Technology, 4800 Oak Grove Drive, Pasadena, CA, USA 91109
‡Erkin.Sidick@jpl.nasa.gov

Abstract: We present an adaptive cross-correlation algorithm for large dynamic range extended-scene Shack-Hartmann wavefront sensing. We show that it accurately measures very fine image shifts over many pixels under a variety of practical imaging conditions.

OCIS codes: (100.5070) Phase retrieval; (110.6770) Telescopes

1. Introduction

The conventional method used in Shack-Hartmann wavefront sensor (SH-WFS) first produces a set of spot images from a point-source, then determines the positions of the centroids of these spot images, and finally retrieves the phase information from the estimates of the offsets between these centroid positions and a set of pre-determined reference positions. When used in a closed-loop wavefront sensing and control system of a telescope, it offers high dynamic range, albeit with a lower wavefront measurement resolution than, for example, the Modified Gerchberg-Saxton (MGS) WFS approach [1]. In some applications of space-based, airborne, and ground-based adaptive optical systems, extended-scene SH-WFS provides some great benefits. Poyneer has reported a technique to obtain an estimate on the sub-pixel shift between two scene-based images [2]. We have developed a new, adaptive cross-correlation (ACC) algorithm to estimate with high accuracy the shift as large as several pixels between two extended-scene images captured by an SH-WFS. It determines the positions of all of the extended-scene image cells relative to a reference cell using an FFT-based iterative image-shifting algorithm. We have tested the shift estimation accuracy of this approach with both point-source and extended-scene images. We also compared its phase estimation accuracy with that of a conventional centroid-finding algorithm, and obtained good agreement between the two approaches. In this paper we describe our algorithm and present some results.

2. Position-finding algorithm for extended-scene SH-WFS

The principle of the conventional point-source image (or spot image) based SH-WFS is to determine the local wavefront tilt from the measurement of the displacement of the focal point of a lenslet array. With an appropriate field stop, a Shack-Hartmann sensor can image extended scenes as well as isolated stars. The most challenging task in extended-scene SH-WFS algorithm is to accurately determine the relative positions between a particular extended-scene sub-image (we refer to it as the test image in this paper) and a reference sub-image, each of which being produced by one element of the lenslet array. In order to develop an algorithm for this task, we worked with a series of spot image data measured with a real SH-WFS system. These data include both a reference frame corresponding to the "flat" state of a controllable mirror and a series of test frames corresponding to some distorted states of the mirror. One engineering group at JPL is also building a deformable-mirror based experimental setup to do some specific extended-scene SH-WFS experiments [3]. However, the experimental aspect of this work is beyond the scope of this paper, and here we limit our description to the detail of the algorithm that we have developed.

The necessary SH extended scene was generated in the following way: A measured point-source spot image, as shown in Fig. 1(a), is selected, and it is convolved with an object scene image as shown in Fig. 1(b). This produced an extended-scene image similar to the one obtainable with an extended-scene SH-WFS, as shown in Fig. 1(c) [3]. A linear detector model is then applied to introduce fixed pattern pixel gain, offset and dark current pattern, as well as Poisson and read-noise processes. For completeness, pixelization, charge-diffusion and quantization effects are also included. The relative locations of the different SH extended-scene sub-images were determined with the following process:

(1) Determine the center coordinates of all of the sub-images in Fig. 1(c), and store these x- and y-coordinate values in a [2x*M*] matrix. In our case, the centroid locations of the spot image in Fig. 1(a) were used for this purpose.

This work was performed at the Jet Propulsion Laboratory, California Institute of Technology, under a contract with the National Aeronautics and Space Administration.

Figure 1. (a) A point source spot-image of a Shark-Hartmann sensor. (b) An object scene image used to create an SH extended-scene image for this study. (c) The SH extended-scene created by convolving (a) with (b).

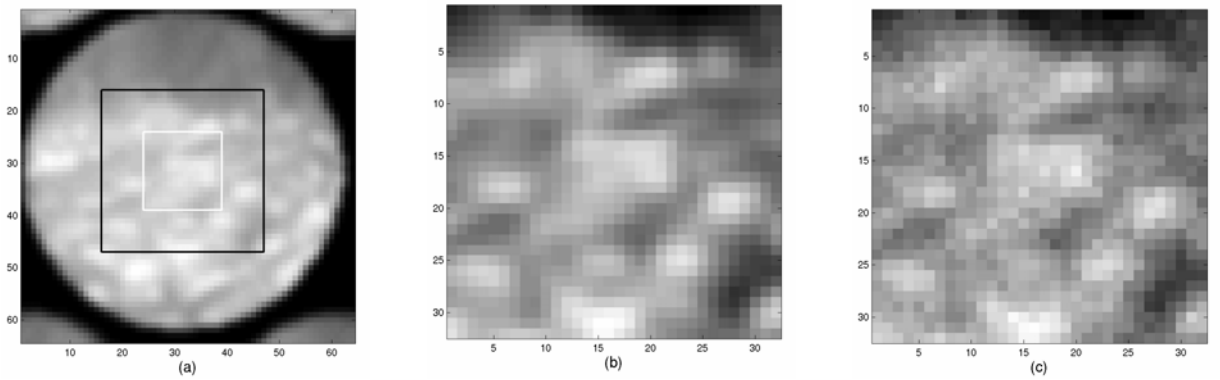

Figure 2. (a) One sub-image of the SH extended-scene. The black-colored box shows a 32x32 pixel (N=32) sub-aperture, and the white-colored one a 16x16 pixel (N'=16) sub-aperture. These sub-apertures are referred to as cells in this paper. (b) A 32x32 cell inside the square black box in part (a) before adding the readout noise. (c) Same as part (b) except the readout noise was added and the dark signal was subtracted from the image.

(2) Choose an NxN pixel sub-aperture within each sub-image with the x- and the y-coordinates determined in Step 1 as its center, as shown with a black box in Fig. 2(a). Such a sub-aperture is referred to as a cell in this paper. Also, choose one cell as a reference cell, preferably near the center of the whole extended-scene image. In the following we use the position variables (x, y) to denote the position dependence of a cell, and use (u, v) to denote the position dependence of the Fourier-transform of a cell. That is, the $r(x,y) \leftrightarrow R(u,v)$ pair represents the reference cell in the original signal and the Fourier domains, respectively. We call all of the other cells as test cells and represent them with the $s_i(x,y) \leftrightarrow S_i(u,v)$ pair. Figures 2(b) and 2(c) show the cell chosen from the sub-image in Fig. 2(a). Among these two figures, part (b) was obtained without adding detector readout noise, and part (c) was obtained by adding readout noise and subtracting the dark signal from the original image. The image in Fig. 2(c) spans the 769 – 1546 range in a 0 - 4095 gray levels. This image is an example of the extended-scene image cells used to test the current algorithm. The dark signal was also created from the same linear detector model by setting the light intensity in all pixels to zero.

(3) Take the central N'x N' pixel portions of $r(x,y)$, where $N' < N$ and both are preferentially a power of 2 for this algorithm, and calculate its FFT (Fast Fourier-Transform). In the example shown in Fig. 2, N=32 and N'=16.

(4) Repeat Step 3 for $s_i(x,y)$. Multiply the two to obtain a cross-correlation function in Fourier-domain, $C_i(u,v) = R^*(u,v)\, S_i(u,v)$, where "*" denotes a complex-conjugate. After that obtain the phase function $\phi_i(u,v)$ of $C_i(u,v)$.

(5) Fit u and v slopes to $\phi_i(u,v)$ over a small (u,v) sub-domain.

(6) Compute $S_i(u,v)$ of the full NxN cell $s_i(x,y)$. Multiply it by the u and v phase slopes obtained in Step 4. After that compute the IFFT (inverse FFT) of this product.

(7) Repeat Steps 4 through 6 in an iteration loop, while cumulating the u and v slopes, until a maximum iteration number is reached or the change in image shift becomes smaller than a pre-determined tolerance.
(8) Repeat Steps 4 through 7 for all $s_i(x,y)$.

3. Performance analysis examples and conclusion

We compared the current algorithm with a conventional centroid-finding method by processing several sets of realistic data. These data included both different strengths of a wavefront error mode, such as focus mode, as well as different types of mirror states. In the simulation, we varied the brightness of an object scene and obtained excellent performance with both the spot-image centroid-finding and the extended-scene ACC algorithms. In Fig. 3, we show the shift estimate accuracy of this ACC algorithm. We obtained these results in the following way: 1) We chose one cell in Fig. 1(c) as the reference cell and the another as a test cell. These two cells had the intrinsic image offsets of Δx = -0.10 and Δy = 0.74 pixels, respectively. The gray-level distributions of these two cells also showed some difference. 2) We generated a series of 9 reference and test cell pairs by varying the maximum number of photons arrived at the detector. In a 0 – 4095 gray-level range, this changed the gray-level range of the reference cell in Fig. 1(c) from 865 – 1155 to 2337 – 3882 before dark subtraction. 3) We shifted each of the 9 test cells by convolution by a known amount along the x-axis, and estimated the image shift with the current algorithm with 3 different tolerance values. Figure 3(a) shows the shift estimate errors, where the error bars represent the standard deviation in shift estimate errors corresponding to 9 brightness levels, and Fig. 3(b) show the average numbers of iterations corresponding to 3 difference tolerance values. As we can see, there is a trade-off between the estimation accuracy and data processing time. Very high accuracy can be achieved when the processing time is not a consideration.

In conclusion, we have developed an adaptive cross-correlation algorithm for a Shack-Hartmann wavefront sensor. It is highly accurate when operating with both point-source images and extended scenes. We expect this algorithm to become widely useful in large dynamic range Shack-Hartmann wavefront sensing and control applications, including the SH systems used in ground and space based telescopes.

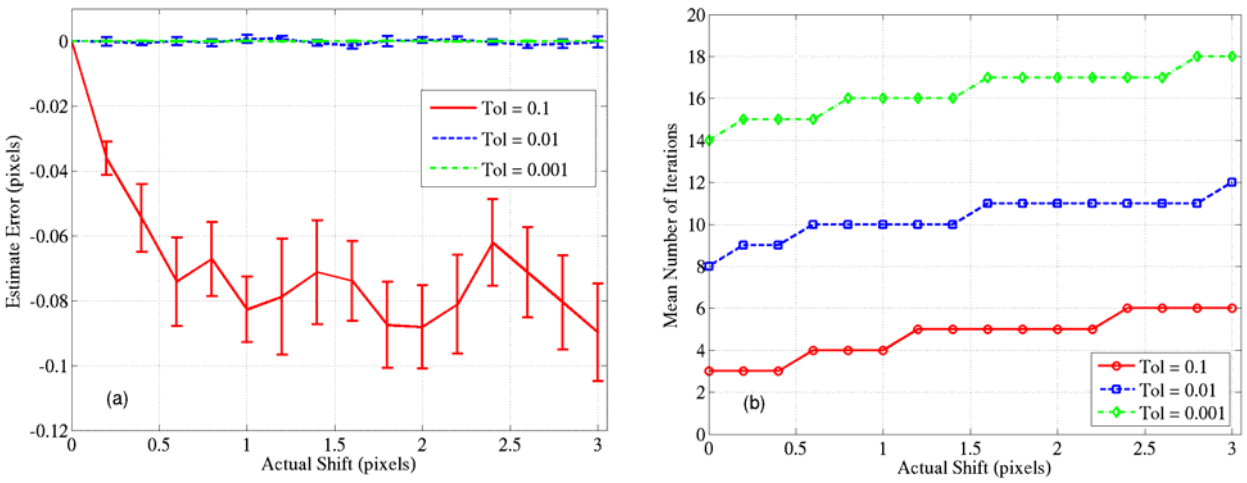

Figure 3. Comparison of (a) estimate errors and (b) total number of iterations corresponding to different image-shifting tolerances. The error bars in part (a) correspond to the standard deviation of estimate errors obtained with 9 different scene brightness levels.

4. References

[1] Scott A. Basinger, David C. Redding, Andrew E. Lowman, Laura A. Burns, Karen Y. Liu, and David Cohen, "Performance of wavefront sensing and control algorithms on a segmented telescope testbed," Proc. SPIE Int. Soc. Eng. 4013, 749 (2000).

[2] Lisa A. Poyneer, "Scene-based Shack-Hartmann wave-front sensing: analysis and simulation," Appl. Opt. 42, 5807 (2003).

[3] Rhonda M. Morgan, Kirill V. Shcheglov, Joseph J. Green, Catherine M. Ohara, Jennifer Roberts, and Erkin Sidick, "Testbed for extended-scene Shack-Hartmann and phase retrieval wavefront sensing," Proc. SPIE Proc. SPIE Int. Soc. Eng. 5903, 59030I (2005).